THE 17th CHESAPEAKE SAILING YACHT SYMPOSIUM

ANNAPOLIS, MARYLAND, MARCH 2005

Sailing Yacht Rig Improvements through Viscous Computational Fluid Dynamics

Vincent G. Chapin
Fluid Mechanics Department, Ensica, FRANCE

Romaric Neyhousser
Aquitaine Design Team, Arcachon, FRANCE

Stéphane Jamme, Guillaume Dulliand, Patrick Chassaing
Fluid Mechanics Department, Ensica, FRANCE

ABSTRACT

In this paper we propose a rational viscous Computational Fluid Dynamics (CFD) methodology applied to sailing yacht rig aerodynamic design and analysis. After an outlook of present challenges in high speed sailing we emphasized the necessity of innovation and Computational Fluid Dynamics to think, validate and optimize new aero-hydrodynamic concepts. Then we present our CFD methodology through CAD, mesh generation, numerical and physical modelling choices and their validation on typical rig configurations through wind-tunnel tests comparisons. The methodology defined, we illustrate the relevance and wide potential of advanced numerical tools to investigate sailing yacht rig design questions like the relation between sail camber, propulsive force and aerodynamic finesse, and like the mast-mainsail non linear interaction. Through these examples, it is shown how sailing yacht rig improvements may be drawn by using viscous CFD based on Reynolds Averaged Navier-Stokes equations (RANS). Then the extensive use of viscous CFD rather than wind-tunnel tests on scaled models for the evaluation or ranking of improved design open the door to time saving.

The last part illustrates on a preliminary study of the Y. Parlier Hydraplaneur double rig how the proposed CFD methodology may be applied to this complex largely unknown rig. We show how it is possible to increase our understanding of his flow physics with strong sails interactions and we hope this will open new roads toward optimized design.

Along the paper, the necessary mutual comparison presented between CFD and wind-tunnel test will be also the occasion to focus on limitations and drawbacks of viscous CFD tools to discuss them and address their future improvements.

NOTATION

AR	sail aspect ratio (b^2/S)
b	sail spanwise length

β_a, β_{AW}	apparent wind angle
β_h	leeway angle
$\beta_a + \beta_h$	wind/water angle in the boat reference frame
C	sail chord
C_d, C_l	drag and lift force coefficients
C_r	propulsive force coefficient
C_h	heeling force coefficient
C_p	pressure coefficient
δ	sail trim angle
d	mast diameter
d/c	non-dimensional mast diameter
ε_a	aerodynamic drag angle
ε_h	hydrodynamic drag angle
f	sail camber
f/c	sail camber ratio
f_a	aerodynamic lift-to-drag ratio
f_h	hydrodynamic lift-to-drag ratio
F_{da}, F_{la}	aerodynamic drag and lift
F_{ha}	aerodynamic heeling force
F_{ra}	aerodynamic propulsive force
F_{ta}	total aerodynamic force
F_{lh}	hydrodynamic side force
F_{dh}	hydrodynamic resistance
F_{th}	total hydrodynamic force
I	aerodynamic angle of attack
S	sail surface
x_{re1}	suction side reattachment point location on the sail
x_{se2}	suction side separation point location on the sail
$//_a$	axis parallel to the apparent wind
$\perp_a$	axis orthogonal to the apparent wind
$//_h$	axis parallel to the boat speed
$\perp_h$	axis orthogonal to the boat speed

INTRODUCTION

Present period is focused on high efficiency and high velocity in numerous domains of activities. High speed sailing yacht agree with this present law. Following this principle, more and more sophisticated computational methods are more and more necessary to increase sailing yacht speed. Actually, wind-tunnel tests on sails and towing-tank tests on hulls and appendages are not sufficient to increase yacht speed. Today, the novelty is that sailing and sailing with the best sailors and the best boats is not sufficient to increase yet sailing yacht speed without using the gigantism road of the No Limit class or the windy road on which windsurfing are again the best!

The 13th November 2004, Yellow Pages sailing speed record falls by Finian Maynard a major concurrent of the windy road on his windsurf with a five hundreds meters speed of 46.82 knots! But to sail at 46 knots a windsurfer need 45 to 50 knots of wind when Yellow Pages just need 20 to 25 knots. This is not the same story.

Besides, this all class sailing speed world record, the No Limit class is the queen of the twenty-four hours sailing speed with nearly 30 knots.

To go further, without gigantism or windy windsurf, high finesse is needed. And high finesse is a double challenge: aerodynamic and hydrodynamic. Facing this challenge, we think two major ingredients will be present in future high speed sailing project:

- Innovation.
- Computational Fluid Dynamics.

It is necessary to develop new aero-hydrodynamic concepts like Hydroptère, Hydra-planeur, double rig, π-sail, etc... It is necessary to develop sophisticated computational models to understand how sail generate thrust without too much heeling moment, how hull and appendages generate drag or thrust, what is the relation between sail shape and sail forces, what is the relation between sail design shape and sail flying shape.

In fact, numerous computational models exist based on more or less radical hypothesis. Widely used models for sailing applications involve inviscid equations (potential flow, lifting-line, lifting-surface, vortex-lattice methods…). These models are computationally efficient, largely diffused and well accepted by the sailing community but the inviscid hypothesis they use is not relevant when flow separation play a significant role in performance evaluation. And this is not only in downwind sailing conditions as is said sometimes. Separated regions and separation bubbles are not only present in downwind sailing conditions but also in upwind sailing conditions. Too much camber generates separation on mainsail or jib as not predicted by inviscid methods. Mast at the leading-edge of the mainsail generates separation bubble (Marchaj 1976, Milgram 1978, Wilkinson 1984, 1989, 1990).

Today, viscous Computational Fluid Dynamics (CFD) is a breakthrough. This is a numerical model which describes the dynamic of fluids around bodies based on the resolution of the complete Reynolds Averaged Navier-Stokes equations (RANS), (Cowles & al. 2003, Graf & Wolf 2002, Jones & Korpus 2001, Caponnetto & al. 1999). For the first time it is possible to obtain reliable results in three-dimensional viscous flow with separated regions and large separation bubbles (Durbin 1995). This will increase our understanding and hence open roads toward better design.

But, there is a cost to obtain this better flow physics understanding. These advanced tools have two major drawbacks. First, they have a relatively high computational cost. Nevertheless, this computing time decreases each year with the always increasing computer power and the recent apparition of multiprocessors personal computers. Secondly, they need high-level expertise and a continuous detailed validation process through wind-tunnel measurements

comparisons to increase our confidence in their results and do the right choice at the right place among the high number of numerical methods and physical models.

In this context, at Ecole Nationale Supérieure d'Ingénieurs de Construction Aéronautique, we try to gather the local aeronautical know-how in Computational Fluid Dynamics to transfer it to the benefit of the sailing community. Also, in this paper, we shall provide detailed flow analysis around mast-sail geometries to validate CFD tools with wind-tunnel tests. We illustrate how to use these tools to improve rig design. And finally, the last part is devoted to a preliminary study on the innovative double rig of Yves Parlier Hydraplaneur with two and three-dimensional RANS simulations. This last part is a good example to put in perspective possible benefits of CFD tools with the aid of sail designers to improve complex rigs with many interacting sails.

COMPUTATIONAL MODEL

In this section, main elements of the computational model are described. First the fluid dynamics equations used are presented then the solver and physical models and limitations are described. The main fact is that we are using viscous Navier-Stokes equations on hybrid meshes with structured and unstructured part in the computational domain with conformal or non-conformal interfaces between domains. This is a powerful technology with high flexibility for mesh generation of interacting sails for two and three-dimensional flows.

Governing equations

Simulations presented in the paper are based on the numerical resolution of the following Reynolds Averaged Navier-Stokes equations:

$$\frac{\partial \rho}{\partial t} + \frac{\partial}{\partial t}(\rho u_i) = 0$$

$$\frac{\partial}{\partial t}(\rho u_i) + \frac{\partial}{\partial x_i}(\rho u_i u_j) = -\frac{\partial p}{\partial x_i} + \frac{\partial}{\partial x_j}[\tau_{ij} + R_{ij}]$$

With the viscous stress tensor

$$\tau_{ij} = 2\mu\,[S_{ij} - \frac{1}{3}\frac{\partial u_k}{\partial x_k}\delta_{ij}]$$

the deformation tensor

$$S_{ij} = \frac{1}{2}(\frac{\partial u_i}{\partial x_j} + \frac{\partial u_j}{\partial x_i})$$

and the turbulent Reynolds stress tensor R_{ij} which should be modelled (see turbulence modelling part). Following Boussinesq hypothesis this tensor may be approximated by:

$$R_{ij} \cong \mu_T\,[S_{ij} - \frac{2}{3}\frac{\partial u_k}{\partial x_k}\delta_{ij}] - \frac{2}{3}(\rho k)\,\delta_{ij}$$

Solver

The software package used to resolve the Navier-Stokes equations is Fluent 6. It is a steady or unsteady, compressible or incompressible, three-dimensional solver which resolve the previously given Reynolds Averaged Navier-Stokes equations. In the simulations presented, we have used the segregated solver and mainly the Spalart-Allmaras turbulence model in its vorticity-based or strain-vorticity-based production term. When not explicitly specified, second-order spatial and temporal schemes were used in the steady version.

To solve the Navier-Stokes equations proper boundary conditions are required on all calculation domain frontiers. At wall boundary, the no-slip condition is applied. A pressure outlet boundary condition is applied at the outlet. A velocity inlet boundary condition is applied on other frontiers (inlet, up and down).

Mesh as a bottleneck

The mesh generation is a crucial step in the process of RANS simulation for many reasons. First of all, it is a time consuming activity which need engineer experience and long practice to rigorously clean the CAD geometry and do the best choice for the mesh topology. Secondly, the mesh influence on results on typical sails configurations is really important and should be carefully evaluated and bounded by relevant choices in mesh size in the important flow regions. Boundary layers have to be well resolved on all bodies (mast and sails) and this impose a critical criterion on mesh size in the normal direction to walls. But this well-known criterion is not enough to have a good flow description and results independent to mesh. All flow gradients have to be well resolved and this is not a simple task on typical sails because of the zero thickness and the subsequent leading-edge pressure gradient when angle of attack is not ideal.

In fact, it is good to say and to know that results are never totally independent to the chosen mesh as opposed to what is frequently argued. The relevant question when interpreting RANS results on sails is: "how bounded is the mesh influence on interesting results".

To illustrate this point, figure 1, we have shown the lift-to-drag ratio convergence with mesh number of points on a typical sail (Wi65: f/c=12.5%, Re = 1.4 x 10^6) calculated on four meshes.

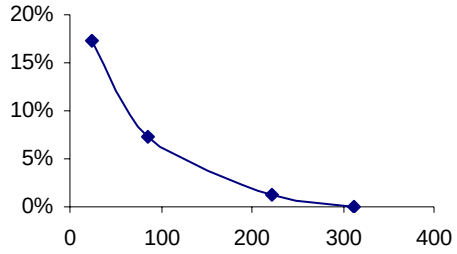

Figure 1: lift-to-drag ratio convergence with mesh refinement (number of points / 1000).

Another important feature of mesh is their adaptability to different kind of geometries. A critical point for yacht rig aerodynamic study is the necessity to generate meshes on multiple bodies (mast, mainsail, jib, etc…) which interact. The challenge is to generate good quality meshes in the boundary layers regions of each body without using too high aspect ratio cells and with a good control in the interaction regions which may be smalls (mainly between mainsail and jib as may be seen on figure 3). To respect these topologic constraints, a good candidate is hybrid meshes (as may be seen on figure 2a, 2b) with eventually non conformal interface between the inner structured region around masts and sails and the outer unstructured region around all interacting structured domains (figure 3). The mast trailing-edge with link to the zero-thickness sail is a region of difficulty for the structured mesh part and need much attention and tricks.

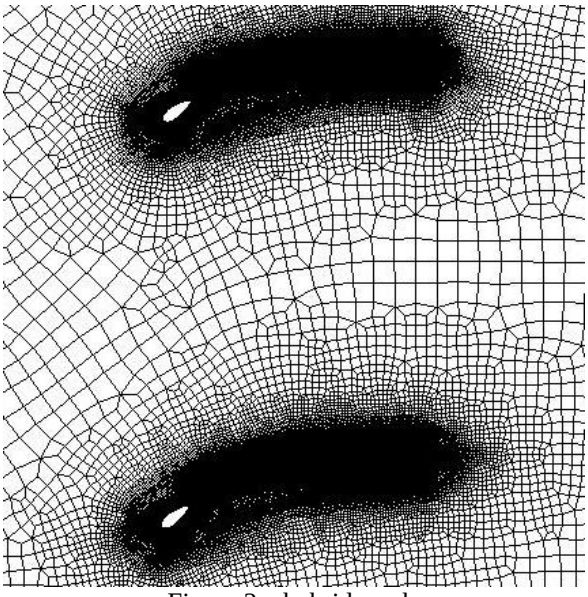

Figure 2a: hybrid mesh.

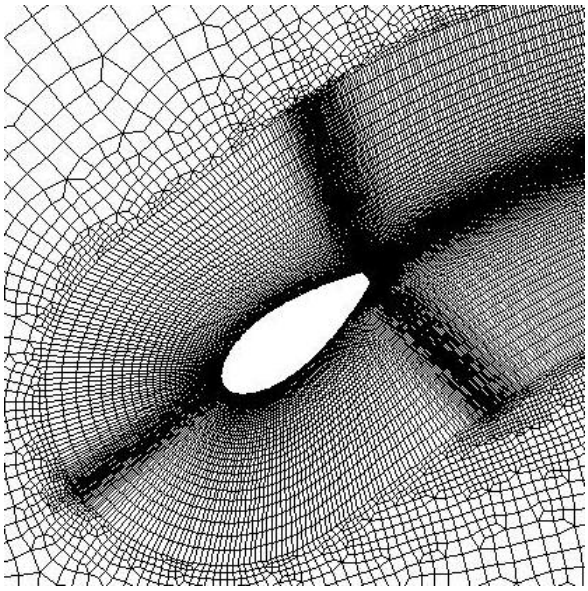

Figure 2b: zoom on a typical hybrid mesh in the mast and sail region.

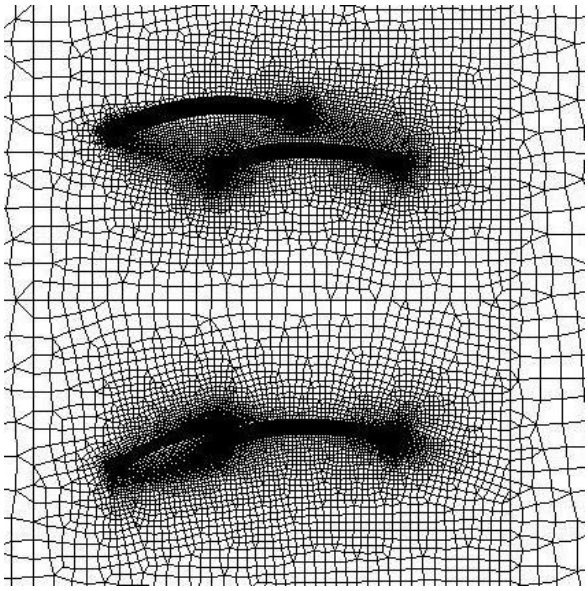

Figure 3: hybrid mesh with four interacting sails.

Transition and turbulence modelling

A reliable prediction of the boundary layer transition through computer simulation is always a challenge today. The transition of a boundary layer is a highly complex physical phenomenon. It is a problem of stability of the Navier-Stokes equations which are highly sensitive to background turbulence level, pressure gradient, surface roughness, etc… The range of existing transition prediction methods extends from simplified empirical relationships through those based on linear stability to direct numerical simulations. All of these methods have critical limitations. No transition models are implemented in RANS simulations. Eventually

transition may be tripped when transition location is known.

In the same time, mast and sail aerodynamic is highly concerned with separation bubble, turbulent transition and turbulent reattachment process and it is well known that these phenomenon and their associated pressure losses may have critical influence on pressure and friction distribution on sails. Also an accurate representation of laminar and turbulent separated flow regions is critical when we are concerned with drag prediction.

Despite this, we will see in this paper that a simple low cost turbulence model like the Spalart-Allmaras one may have coherent qualitative behaviour on mast-sail geometries and may reveal to be better than more sophisticated ones.

The Spalart-Allmaras turbulence model used is a one equation model with standard coefficients values. The equation is a transport equation for the turbulent viscosity as follow:

$$\frac{\partial}{\partial t}(\rho\tilde{\nu}) + \frac{\partial}{\partial x_i}(\rho\tilde{\nu}u_i) = P + Diff - Diss$$

$$P = C_{b1}\rho\tilde{S}\tilde{\nu}\,,\ \tilde{S} \equiv S + \frac{\tilde{\nu}}{\kappa^2 d^2} f_{\nu 2}\,,\ f_{\nu 2} = 1 - \frac{\chi}{1+\chi f_{\nu 1}}$$

$$Diff = \frac{1}{\sigma_\nu}[\frac{\partial}{\partial x_j}[(\mu+\rho\tilde{\nu})\frac{\partial\tilde{\nu}}{\partial x_j} + C_{b2}\rho(\frac{\partial\tilde{\nu}}{\partial x_j})^2)]$$

$$Diss = C_{w1}\rho f_w(\frac{\tilde{\nu}}{d})^2$$

$$\mu_T = \rho\tilde{\nu}f_{\nu 1}\,,\ f_{\nu 1} = \frac{\chi^3}{\chi^3 + C_{\nu 1}^3}\,,\ \chi = \frac{\tilde{\nu}}{\nu}$$

$$S_{vorticity-based} \equiv \sqrt{2\Omega_{ij}\Omega_{ij}}\,,\Omega_{ij} = \frac{1}{2}(\frac{\partial u_i}{\partial x_j} - \frac{\partial u_j}{\partial x_i})$$

$$S_{strain-vorticity-based} \equiv |\Omega_{ij}| + C_{prod}\ \min(0, |S_{ij}| - |\Omega_{ij}|)$$

$$C_{prod} = 2\,,|\Omega_{ij}| \equiv \sqrt{2\Omega_{ij}\Omega_{ij}}\,,|S_{ij}| \equiv \sqrt{2S_{ij}S_{ij}}$$

$$f_w = g[\frac{1+C_{w3}^6}{g^6 + C_{w3}^6}]^{1/6}\,,g = r + C_{w2}(r^6 - r)\,,r = \frac{\tilde{\nu}}{\tilde{S}\kappa^2 d^2}$$

$$C_{b1} = 0.1355, C_{b2} = 0.622, \sigma_\nu = 2/3, C_{\nu 1} = 7.1$$

$$C_{w1} = \frac{C_{b1}}{\kappa^2} + \frac{1+C_{b2}}{\sigma_\nu}, C_{w2} = 0.3, C_{w3} = 2.0, \kappa = 0.4187$$

RESULTS

2D RANS validations

Before using viscous RANS simulation tools like Fluent with confidence, to do parametric analysis of sails design variables, preliminary validations are necessary. These tools are complex. They imply modelling, numerical, physical choices during the overall simulation process. Each of these choices must be carefully done through validated background experiences and a well known of the flow physics present in the considered geometries. There are numerous hypotheses hidden behind each choice during geometry CAD design, mesh generation, numerical parameters used, boundary conditions used, etc… These choices will have consequences on convergence properties of the numerical model and on the quality of the results.

Sails aerodynamic is a particularly difficult domain because of the soft nature of sails. The design shape is not the flying shape. The flying shape equilibrium results from the aerodynamic loading of the design shape which should take into account the rigidity of the complete rig including mast, spreaders and riggings. This flying sail shape is solution of a non linear fluid-structure coupling problem.

In this paper we have done the hypothesis that we simulate the flow around the equilibrium flying shapes without taking into account sail deformation. Doing that we may increase our sail flow physics understanding and investigate the effect of design parameters on resultant flying shapes. Besides, it will not be possible to say how to design a sail to obtain the desired flying shape for a given rig.

The fact that sails are not rigid increases the difficulty of the validation process of numerical tools through comparisons with wind-tunnel tests. In the computational model, as said before, we are working with flying shape but in the wind-tunnel, we put design shape which results in a particular flying shape which depends on the wind velocity used and on the rigidity of the scaled rigging used. In this approach, validation are only possible if flying shape are photographed and transformed into a numerical equivalent flying shape through photometry to be used in the computational model.

In this process, there is no perfect solution. A possible solution is to simplify this tricky validation process by using rigid sails to limit their deformation in the wind. When possible, it is the solution we have used to do wind-tunnel test and subsequent mutual validations through comparisons with RANS simulations.

Wilkinson wind-tunnel tests

Up to now, Wilkinson's experimental data-base obtained in the 2.13x1.52m wind tunnel of Southampton University remains the basis to understand the differences between experimental measurements and numerical predictions around mast-sail configurations. To our knowledge, it is the only experimental database in open literature that contains mast and sail pressure distributions for a large number of configurations (with various sail camber and mast diameter). It gives local wall-pressure measurements along the mast and the sail. This local physical information is highly useful to investigate which physical phenomena are captured by the numerical model used (mesh, turbulence model, RANS or URANS equations …).

Wilkinson has shown that in the ranges explored for the parameters (7.5% < f/c < 17.5%, 4% < d/c < 17%, 3.5 10^5 < Re < 1.6 10^6, 2.5° < i < 10°), "*all of the apparently different pressure distributions shapes observed during testing were in fact just forms*" around the universal pressure distribution presented in Figure 4. This universal pressure distribution is divided in nine regions representatives of a particular physical-flow phenomenon as described in the Table of Figure 4. Given this database, a first objective was to measure the RANS simulations capabilities to capture main flow features around Wilkinson's mast-sail geometry. We have chosen two Wilkinson's mast-sail configurations upon which RANS calculations were conducted. In Figure 5, we present a flow visualization from a RANS calculation around the first case with a mast diameter d/c=10% and a camber ratio f/c = 12.5%. Captured recirculation regions on sail suction and pressure sides are clearly seen behind mast separation points. Comparison of Figures 5a and 5b shows that the shape of the upper-surface bubble is similar to those found in wind-tunnel test by Wilkinson (1990) and that the reattachment process of the upper-surface bubble is qualitatively well reproduced by the simulation, with a laminar separation over the mast, a high increase of the turbulent viscosity ratio in the following shear layer and a turbulent reattachment on the sail, where the experiment found a laminar separation followed by a bubble transition and a turbulent reattachment (figure 5).

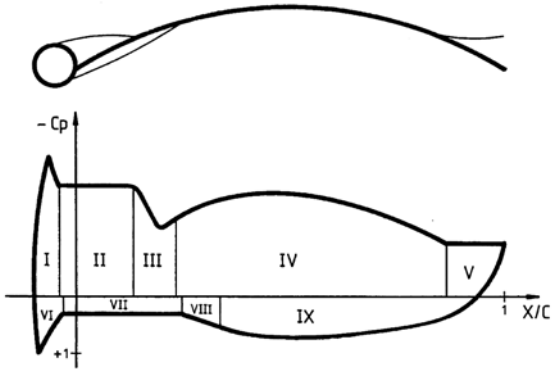

REGION	DESCRIPTION
I	Upper Mast Attached Flow Region
II	Upper Separation Bubble
III	Upper Reattachment Region
IV	Upper Aerofoil Attached Flow Region
V	Trailing Edge Separation Region
VI	Lower Mast Attached Flow Region
VII	Lower Separation Bubble
VIII	Lower Reattachment Region
IX	Lower Aerofoil Attached Flow Region

Figure 4: Universal pressure distribution (from Wilkinson 1984).

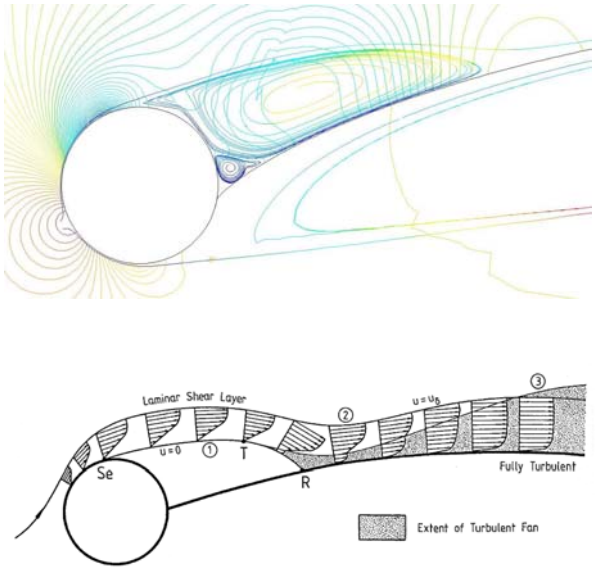

Figure 5: (a) RANS flow visualization (d/c=10%, f/c=12.5%, i=5°, Re=1.4 x 10^6). (b) Upper-surface.

Figure 6 shows comparisons between RANS calculations and Wilkinson results for the pressure distributions. They are very similar despite the complexity of the flow with mast and sail separations, recirculation regions and a change in the flow regime inside the upper-surface bubble region. RANS calculations found the same nine regions proposed by Wilkinson (1989) in Figure 4. Higher differences between experiments and RANS simulations are concentrated in separated-flow regions II and III (upper separation bubble and upper reattachment region) and in region V (trailing-edge separation). Attached-flow regions I, IV, VI and IX (upper and lower mast and sail attached-flow regions) are well predicted. The pressure level of the upper-surface bubble region is well predicted but, as found also by Caponnetto (1998), the bubble length is always underestimated.

Quantitative measurements of the upper-surface-bubble reattachment location and trailing-edge separation point were obtained by Wilkinson (1990) through a finely designed robotic system able to acquire velocity profiles in sail boundary layers. These values and RANS predictions are reported in Figure 7 for comparisons. A flow description of separated regions captured by RANS simulations is presented in figure 8.

Extensive investigation on the upper-surface reattachment location with mesh properties, numerical scheme and turbulence model used have shown that this point is highly sensitive to the computational model properties. Also this region must be carefully taken into account during the mesh generation process, numerical and physical models choices.

Later when RANS simulations are used to make comparisons between different mast and sail geometries, exactly the same computational model should be used to be relevant.

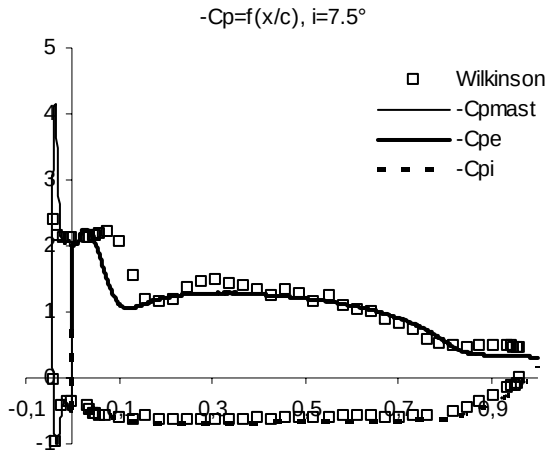

Figure 6: Pressure coefficient distribution –Cp=f(x/c). Comparison of RANS results and Wilkinson wind-tunnel results.

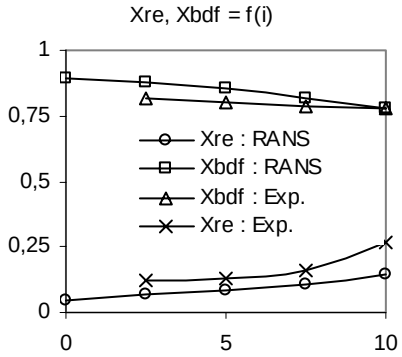

Figure 7: (a) Upper-surface bubble reattachment point and trailing edge separation point versus incidence angle.

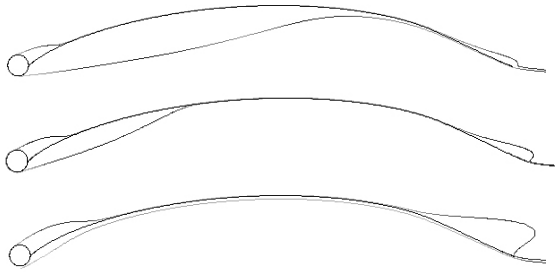

Figure 8: Separation streamlines versus wind angle of attack. (a) i=2.5°, (b) i=5°, (c) i=10°.

Scheme order

In previous part, we have shown elements of validation. This continuous effort of comparisons is necessary to know and increase the domain of predictability of RANS simulations.

To illustrate this fundamental point, let us have a look to a simple validation test about two-dimensional RANS simulations around gennaker profiles of camber ratio ranging from 5% to 30%. The question is to know the maximum lift coefficient accessible to each gennaker profile. Figure 9 show the evolution of this maximum lift coefficient with camber ratio obtained with two different numerical schemes (O1: first order, O2: second order). The result is clear and identical with both numerical schemes. The maximum lift coefficient increase with camber ratio and seems to attain a maximum value with the highest camber ratio value 30%. First order scheme is cheaper in computing time than second order one. But, is this result sufficient to consider first order scheme as a good candidate for simulations around sails? Definitely no! If you are interested in drag prediction, first order scheme is not a good candidate. How to demonstrate this? Just look the prediction of the maximum lift-to-drag ratio of the same gennaker series with same first and second order numerical schemes. Figure 10 give the result. First order results are wrong. Second order results are qualitatively agreed with wind-tunnel tests (Figure 11). Both predict an optimum camber ratio value around 10% between 5% and 15%.

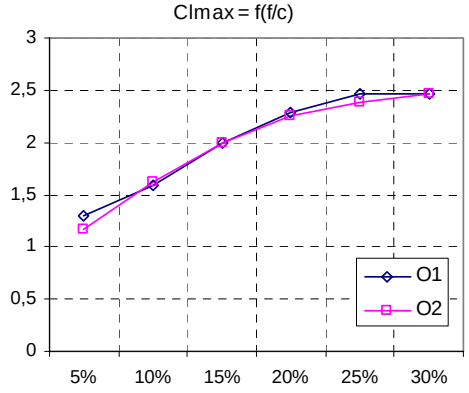

Figure 9: RANS prediction of maximum lift coefficient of a gennaker series of camber ratio ranging from 5% to 30%.

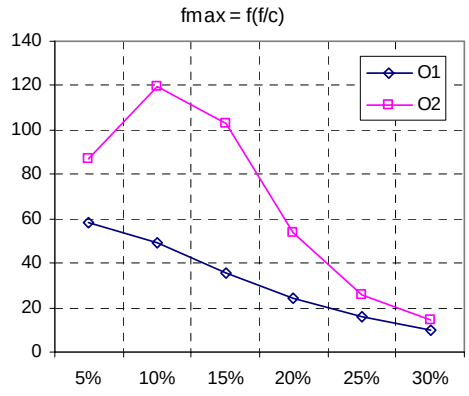

Figure 10: RANS prediction of maximum lift-to-drag ratio of a gennaker series of camber ratio ranging from 5% to 30%.

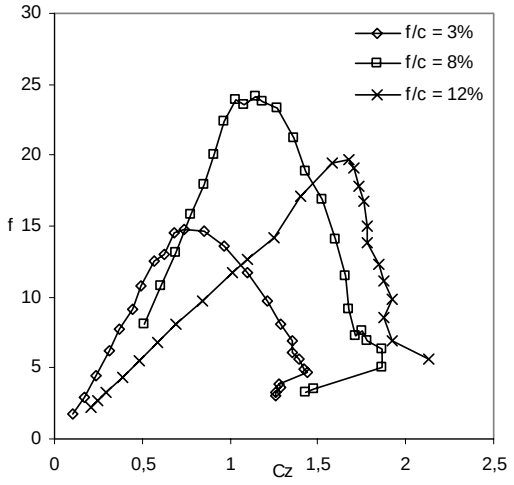

Figure 11: wind-tunnel tests on sails of variable camber ratio.

Turbulence model

Our work has shown that Spalart-Allmaras turbulence model is the best choice. This model is cheaper than other models in CPU time and give more realist turbulent field around mast-sail geometries. As an example, this model doesn't create artificial turbulence production around mast stagnation point as k-ε or k-ω models do.

The major identified problem about turbulence model to capture main features of these separated flow is the upper-surface bubble length prediction and the related drag evaluation for high mast diameter ratio d/c has emphasized by Wilkinson's test case n°52 with d/c=10%. Wilkinson wind-tunnel tests give an upper-surface bubble length of 0.31 and best RANS solution predict 0.16 (table 1). Clearly, this is a difficult task because the flow separate on the mast then develop a laminar shear layer before to transition to turbulence just before to reattach on the upper-sail surface. As said before, there is no transition model in the computational model. Hence turbulence model is not the major problem in the sense that differences between models proposed in Fluent have minor influence on global results and bubble length prediction. They are all wrong from this point of view! Besides that, the trailing-edge separation location seems reasonably well predicted by all turbulence models (table 1).

Paper	Wi 52	Present
Method	Exp.	RANS
x_{re1}	0.31	0.16
x_{se2}	0.82	0.83

Table 1: Upper-surface bubble length and trailing-edge separation location (Wilkinson n°52: d/c=10.2%, f/c = 12.5%. angle of attack i = 5°).

From the turbulence model point of view, last simulations have given the best results about bubble length. With the strain-vorticity-based production term in the Spalart-Allmaras model we found a reattachment location at x_{re1} = 0.20 to be compared to the 0.16 value obtained with the standard vorticity-based production term of the model.

Sail camber and performance

Sailors know that sail camber is a crucial design parameter to choose the best compromise between power and finesse following sea state and wind conditions. Inviscid methods are known to predict continuous increase of sail lift-to-drag ratio when camber increases (Jones & Korpus, 2001). Good sailors know that this is wrong, a limit exist because of flow separation (Bethwaite, 1996). The problem is not simple because bubble and flow separation are non linear phenomena and depend to a lot of design parameters and sailing conditions. To better design complete rigs, we need a tool able to predict limits of finesse increase with camber increases. We will show than viscous RANS based simulation may be the right tool to do that.

Optimum sail camber ratio: to emphasized the leading role of aerodynamic finesse, before going to RANS results, we briefly show through aero-hydrodynamic forces equilibrium equations why it is important to maximize aerodynamic finesse for a given lift coefficient.

If we look at the aero-hydrodynamic forces equilibrium with a no-heel hypothesis (Figure 12), we can write the following relations (Marchaj 1962):

$$F_{lh} = F_{ha}$$
$$F_{dh} = F_{ra}$$

which is equivalent to

$$\beta_a+\beta_h = \varepsilon_a+\varepsilon_h \equiv \mathrm{Arctg}(1/f_a)+\mathrm{Arctg}(1/f_h) \quad (1)$$
$$F_{ta} = F_{th}$$

with f_a the aerodynamic finesse and f_h the hydrodynamic finesse defined by:

$$f_h \equiv F_{lh} / F_{dh}$$
$$f_a \equiv F_{la} / F_{da} \equiv C_l / C_d$$

and β_a the apparent wind angle, β_h the leeway angle. Then, with the aero-hydrodynamic equilibrium we can write

$$f_h \equiv F_{lh} / F_{dh} = F_{ha} / F_{ra} \equiv C_h / C_r$$

and relations between the aerodynamic coefficients (C_l, C_d) and the propulsive and the heeling force coefficients (C_r, C_h) can be written:

$$C_r = C_l \sin(\beta_a+\beta_h) - C_d \cos(\beta_a+\beta_h)$$

$$C_h = C_l \cos(\beta_a+\beta_h) + C_d \sin(\beta_a+\beta_h)$$

When the speed, of a displacement sailing yacht increases, the hydrodynamic drag F_{dh} increases more rapidly than the hydrodynamic lift F_{lh} which increases with the yacht speed square. Hence, the hydrodynamic finesse $f_h = F_{lh} / F_{dh}$ decreases with the yacht speed increase. Also, because the equilibrium equation (1) is verified, for a given water / wind angle $\beta_a+\beta_h$, the yacht speed increases only if the aerodynamic finesse increases. Also, for a given sailing yacht, the higher may be the aerodynamic finesse f_a, the higher may be the yacht speed. From this equilibrium consideration, for a given value of the water/wind angle $\beta_a+\beta_h$, there is a relation between the maximum aerodynamic finesse and the maximum yacht speed.

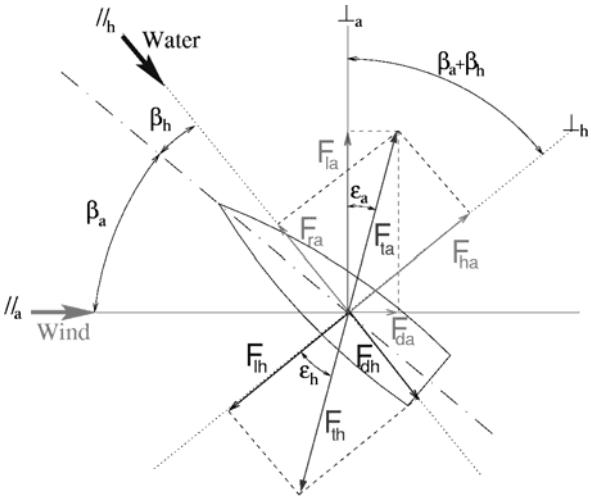

Figure 12: aero-hydrodynamic forces equilibrium in the horizontal plane.

To evaluate the capability of viscous RANS simulations to predict real camber effect on finesse, we have chosen a typical mast-sail configuration with mast diameter ratio d/c=5% and a camber range from 3% to 16%. It is clearly seen figure 13 that in this particular case, the 12% camber sail have the maximum lift-to-drag ratio. We also see that the best camber choice will depend on the lift coefficient value used to equilibrate the hydrodynamic part of the yacht. The importance of this optimum camber prediction is not its value but the fact that an optimum is found. This RANS based simulation capability is of great value for better rig design compared to classical inviscid methods which predict continuous increase of lift-to-drag ratio with camber (Jones & Korpus 2001).

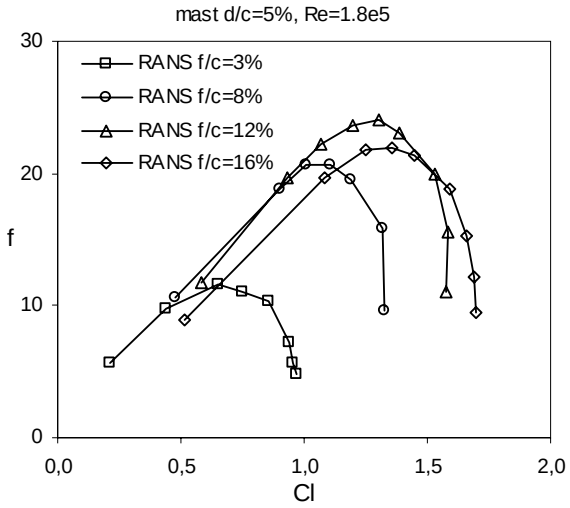

Figure 13: Optimum camber of mast-sail geometry.

At ideal incidence angle (points of maximum lift-to-drag ratio on previous figure), we present the pressure distribution of each sail camber on figure 14. We see the evolution of main flow features with camber value (upper-surface bubble length and base pressure, suction dome amplitude, lower-surface bubble length and base pressure).

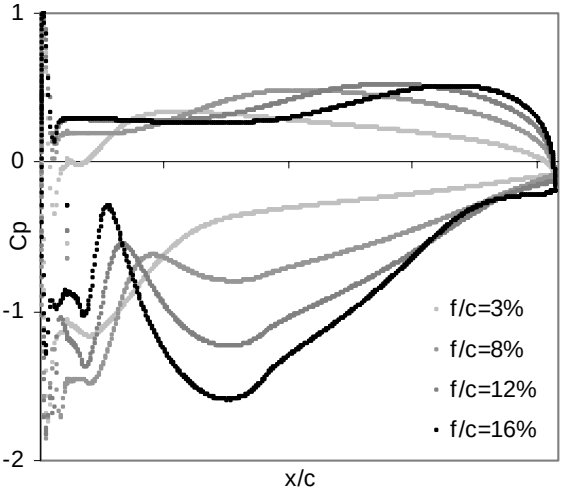

Figure 14: RANS prediction of the sail camber ratio effect on pressure coefficient distribution (d/c=5%, $i=i_{opt} = 4°$).

Mast – mainsail interaction

Main numerical flow analyses done in upwind sailing conditions are done without taking into account mast at the leading-edge of the mainsail or by adding to the sail drag a supplementary parasitic drag of the mast alone in a free stream. This practice is wrong as shown by wind-tunnel tests of Milgram 1978. Hence, a question rises: Does RANS based simulations able to predict the non linear interaction between mast and sail? To investigate this question,

we have done RANS simulations and wind-tunnel tests around a sail with and without a mast. RANS results are given on figures 16, 17, wind-tunnel results on figure 15, 18. It may be seen that the interaction is non linear. If we pose the following drag and lift coefficients decomposition:

$$C_{L\_mast-sail} = C_{L\_sail} + C_{L\_interaction}$$
$$C_{D\_mast-sail} = C_{D\_mast} + C_{D\_sail} + C_{D\_interaction}$$

We may evaluate the interaction term based on RANS and wind-tunnel tests results. These terms are presented for lift coefficient in figures 19 for wind-tunnel tests and 20 for RANS results as a percentage of the mast-mainsail lift coefficient. The same may be done for the interaction drag coefficient. We see that the interaction lift coefficient behaviour is nearly the same for wind-tunnel and RANS results. The interaction term is not negligible mainly for small incidence angles. This is important from a sailing point of view because this correspond to high lift-to-drag ratio points which are useful for upwind sailing. We also see on figure 19 that the interaction term increases rapidly with mast diameter ratio d/c. This is particularly important for high mainsail sections where the sail chord c decrease with d nearly constant.

From this study we may conclude that it will be interesting to include these mast-sail interaction term in lift and drag coefficient evaluation in Velocity Prediction Program (VPP). As shown here, these terms may be evaluated by RANS simulations to derive an approximate model for mast non linear interaction in advanced VPP. For a high quality VPP aerodynamic and hydrodynamic models description, see Van Oossanen, 1993. This may be critical to better take into account the non linear mast effect on sailing yacht performances and perhaps will change rig design trade off about mast.

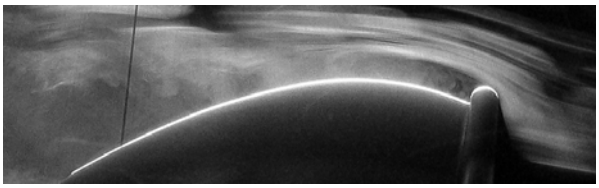

Figure n°15: wind-tunnel test of mast-sail configurations (f/c=12%, d/c=5%, i=10°).

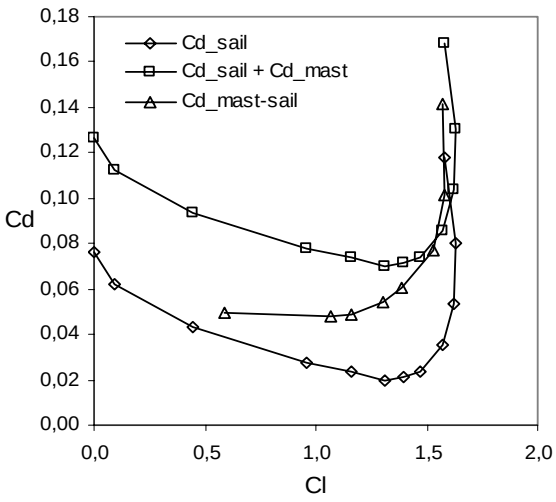

Figure 16: polar of the mast-sail non linear interaction (RANS results).

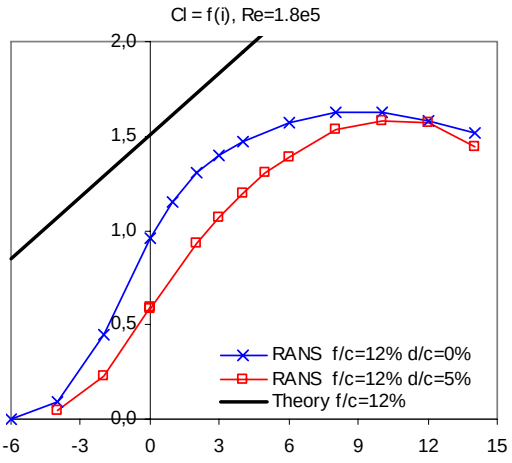

Figure n°17: lift coefficient curve of the mast-sail non linear interaction (RANS results).

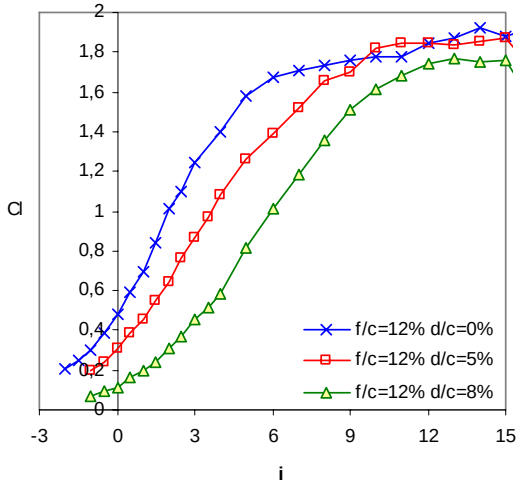

Figure n°18: lift coefficient curve of the mast-sail non linear interaction (Wind-tunnel tests).

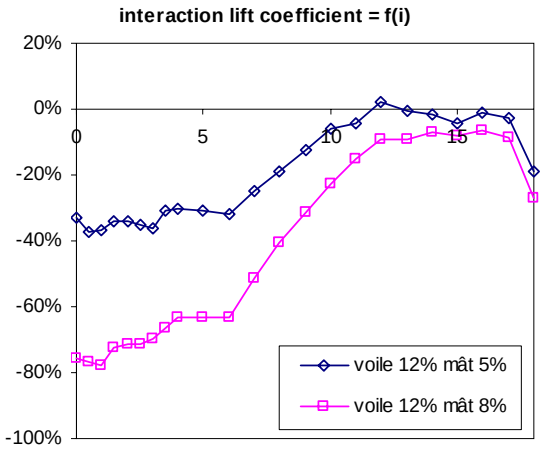

Figure 19: mast-sail non linear interaction and the related lift interaction term (Wind-tunnel tests).

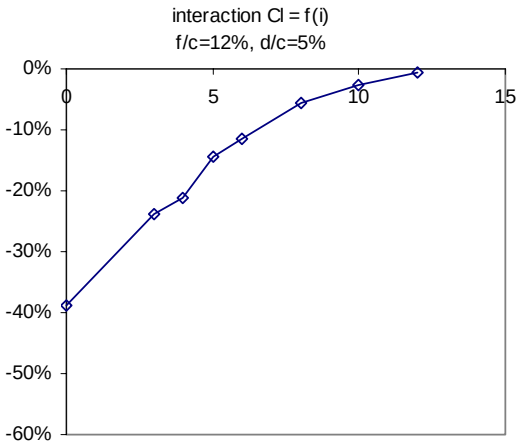

Figure 20: Mast-sail non linear interaction and the related lift interaction term (RANS results).

RANS optimized double rig

We think now that RANS based simulations are mature to play a central role in design decision making before to go to fine tune on real yacht in real wind. They may help to win precious time to sail with tuned yacht rather than to tune basics things on water. This should be particularly true in the study of complex rigs with many sails and masts interacting. To illustrate this point, ENSICA Fluid Mechanics Department has opportunity to bring his contribution to the innovative Yves Parlier's project: the Hydraplaneur. It is a new 60' ocean racing multi-hull (central figure on page 1). To sail faster, this boat is a catamaran to be lighter, with stepped hulls to glide, and a double rig to increase propulsive force without heeling moment penalty.

The Hydraplaneur double rig is a new rig concept to optimize with multiple interacting sails (two mainsails, two wingmasts and eventually two fore sails). The challenge of this boat is to be able to sail sufficiently fast to avoid that the leeward rig may be masked by the windward rig in abeam apparent wind conditions.

In this part, we will illustrate how RANS simulations may be a relevant tool to increase our understanding of the double rig and optimize it in all sailing conditions. The first part is devoted to differential loading, the second one to coupling phenomena and the last one to show first three dimensional simulations on Hydraplaneur rig.

Differential loading on double rig

Here we just want to show that RANS may be complementary to wind-tunnel to increase our understanding of the flow in this double rig to guide future optimization. To investigate the double rig concept, wind-tunnel tests has been done to compare simple and double rig (figure 22) in S4, an open 3x2m elliptic wind-tunnel test section of ENSICA Fluid Mechanics Department (figure 21).

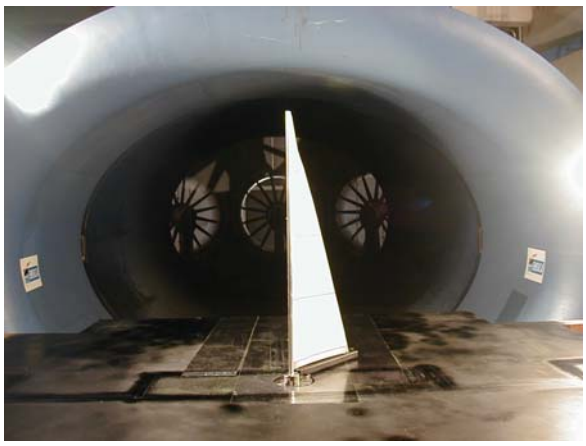

Figure 21: S4 wind-tunnel test section in aero-dynamic sail force measurements configuration.

Forces and moments measurements give us precious quantitative information about the relative propulsive potential of simple and double rig as a function of the apparent wind direction. A major limitation of wind-tunnel tests was the global aerodynamic force measurements which doesn't give us differential loading between windward and leeward rigs. Because this was not sufficient to clearly understand conditions of interaction between windward and leeward rigs, we have done RANS simulations with this aim. One major advantage of numerical simulations is the possibility to decompose drag and lift contributions of each surface individually. Simulations have shown a differential loading between windward and leeward rigs. In fact, these simulations open roads toward innovative sail concepts which will not be developed here.

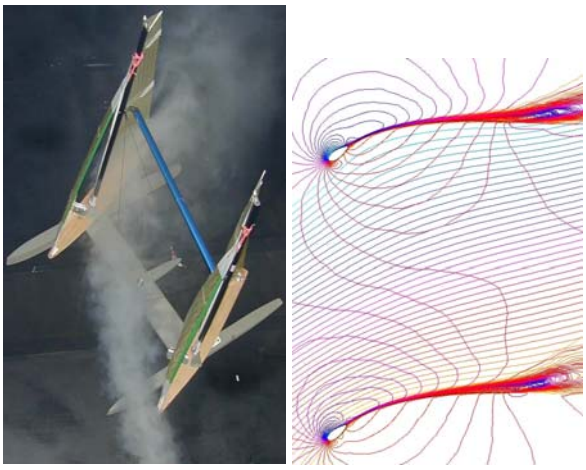

Figure 22: (left) wind-tunnel flow visualization on Hydraplaneur double rig, (right) streamlines, pressure coefficient and turbulent intensity on double rig mid-height cut in upwind sailing conditions β_{AW}=25°.

Coupling phenomena

To illustrate the potential of viscous CFD on complex rig, we consider Hydraplaneur double rig with two mainsails and two fore sails in running conditions with an apparent wind angle β_{AW} = 66°. With this kind of complex rig with many interacting sails, it is highly difficult to determine the right trim angle of each sail to maximize propulsive force for example. In fact, propulsive optimization of these configurations depends not only on trim angles but also sail camber, position of camber, entry and exit angles, etc… As a first illustration about the complexity of the optimization process, we choose a crude configuration as depicted on figure 23.

An analysis of this running configuration show that the windward fore sail is separated from its leading-edge. A consequence of this massive separation is a dead zone of fluid behind him which generate a poor highly turbulent and unsteady flow in the leeward mainsail with a highest mean pressure on the suction face than on the pressure face!

To limit the separation of the windward fore sail, the sailor reflex is to ease its sheet. It is the second configuration presented on figure 24. In this case, we see that the separation is smaller, the dead zone is smaller and the leeward mainsail is better adapted to the flow. But, another direct consequence of that change of the fore sail trim angle is a new separation on the windward mainsail which in turn should be trimmed and so on toward the right choice of all parameters. In fact, all sails are coupled through the pressure field and viscous separation zones. The sail design and tuning in these complex configurations will be probably a tricky task. Sail design and optimization based on viscous CFD should be a precious tool to do a better work before to cut and try adapted new sails.

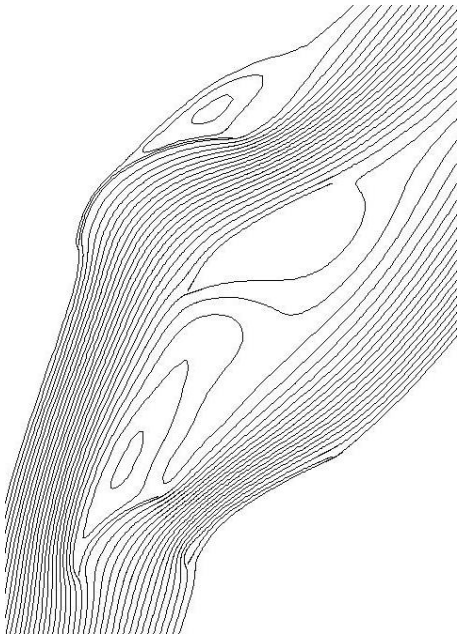

Figure 23: viscous streamlines at mid-height cut in a four sails configuration for running with windward fore sail angle of attack i_{f1}=15°.

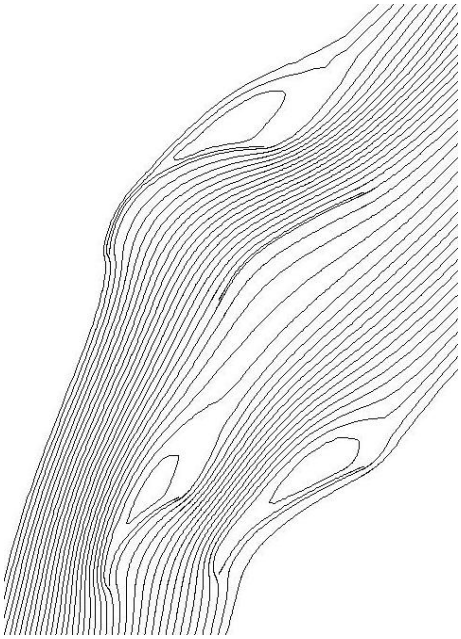

Figure 24: viscous streamlines at mid-height cut in a four sails configuration for running with windward fore sail angle of attack i_{f1}=8°.

Three-dimensional simulations

First investigations of the three-dimensional flow field around Hydraplaneur double rig have been done. Geometry used includes two wingmasts, two mainsails and eventually arms of the boat. Two flow conditions were used with 15 knots of true wind. The first one corresponding to upwind sailing conditions with an apparent wind angle of 25° and the second one to reaching conditions with an apparent wind angle of 65°. Upwind simulations were done without

atmospheric boundary layer in this first stage. In reaching conditions, a turbulent atmospheric boundary layer profile is used with apparent wind gradient and apparent wind angle gradient following:

$$V_{TW}(z) = V_{TW}(z_{ref})[z / z_{ref}]^{1/7}$$

$$\beta_{AW}(z) = Arctg[\frac{V_{TW}(z)\sin\beta_{TW}}{V_B + V_{TW}(z)\cos\beta_{TW}}]$$

Actually, it is relatively easy to take into account the wind vertical gradient in three-dimensional RANS based simulations through an inlet boundary condition with a specified velocity profile. Investigations of the influence of the atmospheric state (laminar or turbulent) on the rig performance will be easy to do. One difficulty is to transport this atmospheric boundary layer profile from the inlet to the boat location in the computational domain without smearing (Figure 25).

Studies have been done to determine relevant choices necessary during mesh generation to capture atmospheric boundary layer with sufficient accuracy. Different mesh topologies were tested during this process to determine the more efficient choice between computing time to obtain a converged solution and accuracy of the wind vertical gradient at the boat location after its transport along the flow domain.

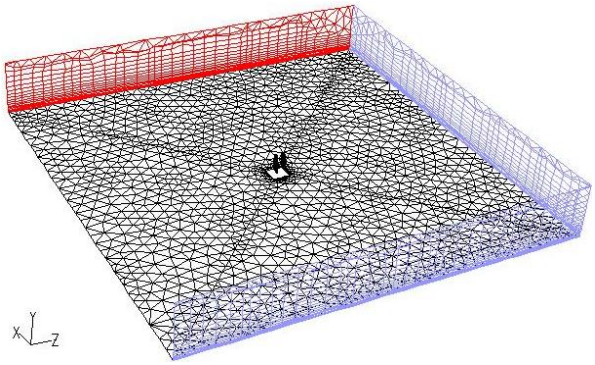

Figure 25: typical three-dimensional mesh with prismatic cells for atmospheric boundary layer transport.

Extend of the computational flow domain was approximately 70 sail chord in both horizontal direction and 3 mast height in the vertical direction (figure 25). Numerous unstructured meshes were generated. In upwind sailing condition, the first coarse mesh used was composed by approximately 544 000 tetrahedral elements with 4 000 cells on arms, 6000 on masts and 30 000 on sails (left figure on page 1). In a second time refined meshes were used to increase masts and sails boundary layer development. The finest one for upwind conditions contain 2 125 000 elements.

A first task assigned to three-dimensional simulations was to measure the three-dimensional character of the flow in this double rig and by consequence, to measure the relevance of preliminary two-dimensional simulations for specific tasks. To illustrate this point, figures 26 and 27 shows the deformation of a streamline plane going through the double rig at the boom height for the first one and at the mid-mast height for the second one. Streamlines are coloured by vertical velocity with a colormap amplitude of +/- 20% of the free stream apparent wind velocity. We see that the three-dimensional character of the flow is more pronounced in the lower part of the rig as we know. The vortical structure of the flow at the boom height is clearly visualized.

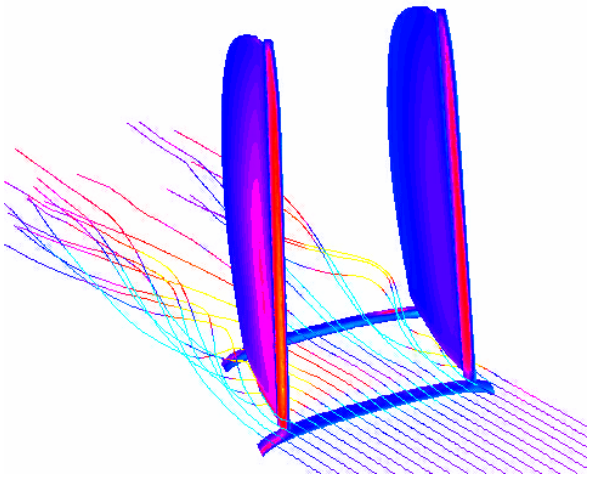

Figure 26: streamlines in the horizontal plane z=2.6m

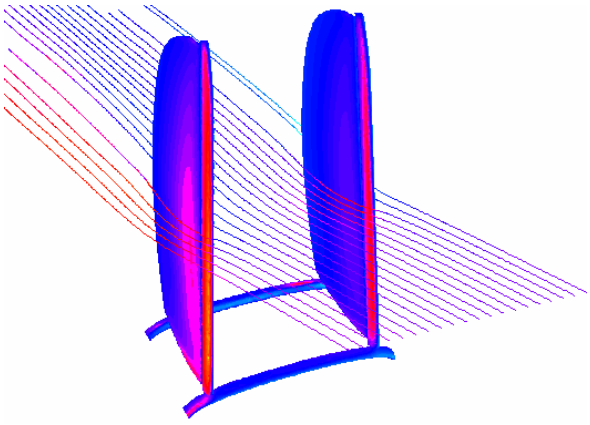

Figure 27: streamlines in the horizontal plane z=12.6m

Figure 28 shows another view of the flow field always in running conditions. Tip vortical structures at both ends of sails in the aft cut plane are always clearly seen on the rear plane coloured by total pressure. We see that the lower vortical structure is stronger than the higher one. An examination of the static pressure field on windward and leeward rigs shows that the leeward rig is more loaded that the windward one. This differential loading results in a

lift coefficient ratio $Cl_{leeward}/Cl_{windward}$ of 1.31 in this attitude. This kind of viscous CFD may be used to better know how to design sails of this double rig. As an example, we may investigate how to equilibrate windward and leeward loading and see if induced drag of the double rig which may be decomposed following this expression:

$$C_{di} = C_{di\_windward} + C_{di\_leeward} + C_{di\_interaction}$$

is really minimized with no differential loading as shown by inviscid lifting-line analysis (von Mises 1959).

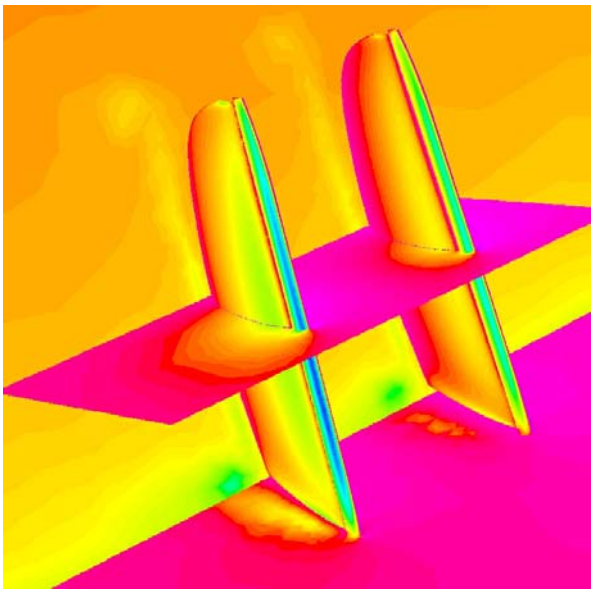

Figure 28: 3D RANS flow visualization of Hydraplaneur double rig in a turbulent atmospheric boundary layer.

CONCLUSIONS

We have proposed a complete CFD methodology to improve sailing yacht rigs. We have shown numerous detailed validations through wind-tunnel tests comparisons to separate easy prediction from more difficult one like suction surface bubble length. We have emphasized the role of the mast at the leading-edge of the mainsail in upwind sailing conditions to produce accurate ranking of the tested rig design. We have demonstrated the capabilities of viscous CFD tools to capture the mast-sail non linear interaction and sail-sail non linear interactions in complex rigs with multiple sails like the Hydraplaneur double rig.

Now extended validations on numerous two-dimensional mast-sail configurations with a range of sail camber and mast diameter ratio have been done and first three-dimensional simulations on complete rigs with atmospheric boundary layer have been done, we planned to investigate two directions: automation of the CFD methodology to tackle two-dimensional optimization problems and three dimensional simulations on complex rigs to increase our sail flow physics understanding to open roads toward clear thinking optimizations and innovations.

But flow in sails is not only flow because sails are not rigid structures. Also, we are aware to the needed development of a fluid-structure coupling strategy to be able to create a link between design shapes and flying shapes.

ACKNOWLEDGMENTS

Authors wish to acknowledge people who have made this work possible: R. Neyhousser from Aquitaine Design Team, F. Haddad for discussions, students B. Haddad, B. Lepine and S. Castanet who have given their contribution. Thanks are also expressed toward J.B. Cazalbou for his help, H. Belloc, V. Allain, S. Lefèvre, G. Busnel and W. Richard for their support on the experimental part and ENSICA for the support of this activity. This research was partly funded by Y. Parlier – Hydraplaneur Médiatis Région Aquitaine project.

REFERENCES

Bethwaite F., “High performance sailing”, Waterline Books, p209, 1996.

Caponnetto, M. and Castelli, A. “America's Cup Yacht Design using Advanced Numerical Flow Simulations”, EPFL Super Computing Review, 10, Nov 1998.

Castanet, S., « Simulation numérique de l'écoulement 2D décollé autour d'un mât et d'une voile » , Rapport de stage de fin d'étude, ENSIAME, 2004.

Chapin V.G., Jamme S., Haddad B., Lepine B., « Ecoulements 2D décollés autour d'un mât et d'une voile », VIIème Rencontre Fluent France, 15-16 Octobre 2003, Paris.

Chapin V.G, S. Jamme, R. Neyhousser, « Aéro-dynamique grand-voile – mât », 2nd Workshop Science & Voile, Ecole Navale, Lanvéoc-Poulmic, Mai 2004.

Chapin V.G., S. Jamme and P. Chassaing, “Viscous Computational Fluid Dynamic as a Relevant Decision Making Tool for Mast-Sail Aerodynamics”, accepted for publication in Marine Technology Jan 2005.

Cowles G., Parolini N., Sawley M.L., “Numerical Simulation using RANS-based Tools for America's Cup Design”, 16th Chesapeake Sailing Yacht Symposium, Annapolis, Maryland, March 2003.

Durbin P., “Separated Flow Computations with the k-ε-v^2 Model”, AIAA J. vol 33(4), 1995.

FLUENT 6.1User’s Manual, Fluent Inc (2003).

Graf K., Wolf E., “CFD investigations and design integration for IACC yachts”, High Performance Yacht Design Conference, Aukland, 4-6 December 2002.

Haddad B. & Lepine B., « Etude expérimentale de l'interaction mât-voile », Rapport de stage de fin d'étude, Ecole Navale, 2003.
Jones & Korpus, “International America's Cup Class Yacht Design Using Viscous Flow CFD”, 15th Chesapeake Sailing Yacht Symposium, 2001.
Marchaj, C.A.. “Sailing Theory and Practice”. McGraw-Hill, 1962.
Marchaj C.A., “A Critical Review of Methods of Establishing Sail Coefficients and Their Practical Implications in Sailing and in Performance Prediction”, 1976.
Milgram J.H., “Section Data for Thin Highly Cambered Airfoils in Incompressible Flows”, NASA CR-1767, July 1971.
Milgram J.H., “Sail Force Coefficients for Systematic Rig Variations”, September 1971.
Milgram J.H., “Effects of Masts on the Aerodynamics of Sail Sections”, Marine Technology, vol. 15(1), 35-42, 1978.
Milgram J.H., Peters D.B., Eckhouse D.N., “Modelling IACC Sail Forces Combining Measurements with CFD”, 11th Chesapeake Sailing Yacht Symposium, 1993.
Milgram J.H., “Fluid Mechanics for Sailing Vessels”, Annual Review of Fluid Mechanics, 30, 613-653, 1998.
Mises R. von, “Theory of flight”, Dover 1959.
Oossanen P. van, “Predicting the Speed of Sailing Yachts”, SNAME Transactions, Vol 101, 337-397, 1993.
Sawley M.L., “Numerical Flow Simulation for America's Cup – A Challenge for Researchers and Students”, EPFL Supercomputing Review, 2002.
Wilkinson S., “Partially separated flows around 2D masts and sails”, PhD Thesis, University of Southampton, 1984.
Wilkinson S., “Static Pressure Distributions Over 2D Mast/Sail Geometries”, Marine Technology, vol 26(4), 333-337, 1989.
Wilkinson S., “Boundary Layer Explorations Over a 2D Mast/Sail Geometry”, Marine Technology, vol 27, 250-256, 1990.